Optimum Battery Size for Fuel Cell Hybrid Electric Vehicle—Part I

Olle Sundström[1]
Measurement and Control Laboratory,
Swiss Federal Institute of Technology,
CH-8092 Zurich, Switzerland
e-mail: olles@ethz.ch

Anna Stefanopoulou
Department of Mechanical Engineering,
University of Michigan,
Ann Arbor, MI 48109
e-mail: annastef@umich.edu

This study explores different hybridization levels of a midsized vehicle powered by a polymer electrolyte membrane fuel cell stack. The energy buffer considered is a lead-acid-type battery. The effects of the battery size on the overall energy losses for different drive cycles are determined when dynamic programming determines the optimal current drawn from the fuel cell system. The different hybridization levels are explored for two cases: (i) when the battery is only used to decouple the fuel cell system from the voltage and current demands from the traction motor to allow the fuel cell system to operate as close to optimally as possible and (ii) when regenerative braking is included in the vehicle with different efficiencies. The optimal power-split policies are analyzed to quantify all the energy losses and their paths in an effort to clarify the hybridization needs for a fuel cell vehicle. Results show that without any regenerative braking, hybridization will not decrease fuel consumption unless the vehicle is driving in a mild drive cycle (city drive with low speeds). However, when the efficiency of the regenerative braking increases, the fuel consumption (total energy losses) can be significantly lowered by choosing an optimal battery size. [DOI: 10.1115/1.2713775]

Keywords: fuel cell vehicle, dynamic programming, hybridization

1 Introduction

There are two main advantages to hybridize a vehicle equipped with a fuel cell system (FCS): (i) Decouple the fuel cell stack from the voltage and current demands from the traction motor to allow the FCS to operate as close to optimally as possible and (ii) recover energy when decelerating and braking through regenerative braking. Although these reasons are identical to the reasons for hybridizing an internal combustion engine (ICE) vehicle, the fuel cell stack operation differs from the operation of an ICE. Fuel cells operate at high efficiencies for a wide range of operating conditions. If not considering the regenerative braking, it is not trivial if and how much a FCS vehicle can benefit from allowing the FCS to operate as close to an optimum as possible.

When hybridizing a power train, it is challenging to size the energy buffer (EB) because the drive cycle [1,2], the control policy [3], and the hardware architecture [4] affect the optimal size. The type and characteristics of the energy buffer used also affect the EB sizing. When increasing the EB size in hybrid electric vehicles, the total vehicle weight increases, which affects the fuel consumption. EB sizing is therefore an important issue to consider when developing hybrid electric vehicles.

In this study, the effects of different lead-acid battery sizes have been analyzed, when the power split is decided through dynamic programming optimizations of the deviations from the optimum state of charge and the hydrogen consumption, for two separate cases: first, when regenerative braking is neglected, and second, when regenerative braking with different efficiencies are considered. This is done to separate the benefits from allowing the fuel cell to operate as optimally as possible from the obvious benefits of regenerative braking. A subset of the battery sizing results were first presented in [5].

When making the decision to include a battery or other energy buffer in the power train, it is important to consider the actual costs of the battery and the added complexity associated with hybridization [1,6]. The prices on fuel cells and batteries vary with time; we will therefore only focus on determining the effects of hybridization on fuel consumption.

Section 2 describes the fuel cell hybrid electric vehicle (FCHEV) model together with the dynamic programming strategy used to control the power split. Section 3 shows the results. Finally, in Sec. 4, a discussion and some conclusions from the results are presented as well as possible future work.

2 Method

To investigate how different battery sizes affect the FCHEV performance, an optimal control approach is used. By using this approach, different sizes are evaluated and compared regarding their optimal performances on known drive cycles. Dynamic programming (DP) [7] is used to optimally control the power split between the FCS and the battery. This section describes the FCHEV model, the DP method, and the drive cycles used to evaluate the component sizes.

The general signal flow during the optimizations is shown in Fig. 1, where v is the speed given by the drive cycles and I_{ref} is the input reference current to the FCS. The two performance variables, the battery's state of charge SoC, and the hydrogen consumption in the FCS W_{H_2}, are used to calculate the cost function for the DP optimization.

2.1 FCHEV Model. The FCHEV model is separated into four components: vehicle, regenerative braking, fuel cell system, and battery pack. This section explains how each component is modeled and how they interact with each other. In this study, the energy losses in the power train, DC motor, inverter, and the DC/DC converter have been neglected. The FCHEV model is a simplified version of the detailed model in [8].

DP complexity is exponential in the number of states in the model. It is therefore crucial to minimize the number of states and the computation time of the model. This is done by approximating fast dynamics as instantaneous and employing nonlinear static

[1]This work was done at the Fuel Cell Control System Laboratory at the University of Michigan, Ann Arbor. Olle Sundström is now affiliated with the Measurement and Control Laboratory at the Swiss Federal Institute of Technology, Zurich.

Submitted to ASME for publication in the JOURNAL OF FUEL CELL SCIENCE AND TECHNOLOGY. Manuscript received May 3, 2006; final manuscript received December 20, 2006. Review conducted by Ken Reifsnider. Paper presented at the IEEE International Conference on Control Applications, October 4–6, 2006, Munich Germany.

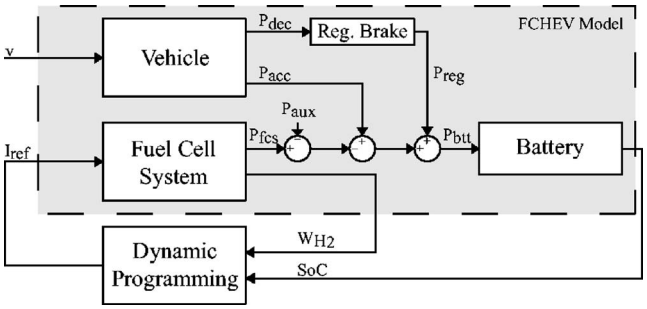

Fig. 1 Fuel cell hybrid electric vehicle components and the signal flow during the dynamic programming optimizations

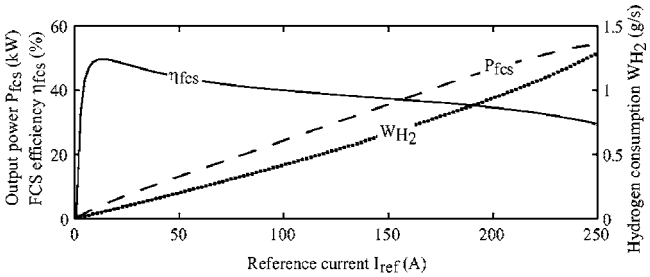

Fig. 2 Fuel cell system output power P_{fcs} (dashed line), hydrogen consumption W_{H_2} (dotted line), and the fuel cell system efficiency η_{fcs}

maps to model their associated steady-state behavior. For example, in the original model [8], the DC/DC converter comprises of second-order system dynamics coupled with a proportional controller that controls the output current from the FCS. In this study, the dynamics of the DC/DC converter are assumed to be fast, and hence, the net current out from the FCS is the same as the DC/DC converter controller current setpoint (input to the DC/DC converter controller).

2.1.1 Vehicle. The vehicle is a midsized car with a mass of 1384 kg, including the FCS and hydrogen storage and excluding the mass of the battery pack. The forces affecting vehicle motion are the output force from the drive train, rolling resistance, and air drag. The power demand P_{dem}, is calculated using the known drive-cycle speeds together with

$$P_{dem}(m,t) = v(t)\{m\dot{v}(t) + F_f(m) + F_d[v(t)]\} \text{ [W]} \tag{1}$$

where the rolling resistance is

$$F_f(m) = K_f mg \text{ [N]} \tag{2}$$

and the air drag is

$$F_d[v(t)] = \frac{\rho_{air} C_d A}{2} v^2(t) \text{ [N]} \tag{3}$$

The acceleration power demand

$$P_{acc}(m,t) = \begin{cases} P_{dem}(m,t) & P_{dem}(m,t) \geq 0 \\ 0 & P_{dem}(m,t) < 0 \end{cases} \text{ [W]} \tag{4}$$

i.e., the positive part of the power demand P_{dem} (1), is provided by the fuel cell system and the battery pack. The deceleration power

$$P_{dec}(m,t) = \begin{cases} 0 & P_{dem}(m,t) > 0 \\ P_{dem}(m,t) & P_{dem}(m,t) \leq 0 \end{cases} \text{ [W]} \tag{5}$$

i.e., the negative part of the power demand P_{dem} (1), is partly absorbed by nonregenerative braking and partly by regenerative braking depending on the regenerative braking efficiency. The road is assumed to be flat, and hence, there is no force from the road grade. The parameters in the vehicle model are shown in Table 1.

2.1.2 Regenerative Braking. The regenerative braking has been modeled as a simple component transferring power associated with deceleration and braking from the wheels to the battery pack. The efficiency of this component, denoted η_{reg}, is varied between 0% and 50% in Sec. 3.2. When regenerative braking is considered, an additional secondary power supply is added to the voltage bus where the FCS and battery pack are connected. The electric power supplied by regenerative braking is

$$P_{reg} = \eta_{reg} P_{dec} \text{ [W]} \tag{6}$$

where P_{dec} is defined in (5).

2.1.3 Fuel Cell System. The FCS is the primary energy source in the vehicle. It converts the energy in the fuel (hydrogen) to electric energy in the vehicle. The hydrogen consumption, shown also in Fig. 2, is calculated using

$$W_{H_2} = \frac{I_{st} n_{cell} M_{H_2}}{2F} \left[\frac{\text{kg}}{\text{s}}\right] \tag{7}$$

where n_{cell} is the number of cells in the stack, M_{H_2} is the molar mass of hydrogen, and F is Faraday's constant. The FCS efficiency, shown in Fig. 2, is defined as

$$\eta_{fcs} = \frac{P_{fcs} - P_{aux}}{Q_{HHV}^{H_2} W_{H_2}} \tag{8}$$

where $Q_{HHV}^{H_2}$ is the energy content of hydrogen (using higher heating value) and P_{aux} is a fixed power demand from all the other FCS auxiliary devices. The current drawn from the FC stack, I_{st}, is calculated using

$$I_{st} = I_{ref} + I_{cm} \text{ [A]} \tag{9}$$

where I_{ref} is the net current out of the FCS and I_{cm} is the current necessary to drive the FC compressor, which is the largest parasitic loss in the FCS and can be calculated as a function of the net current from the detailed model in [9]. Specifically, the I_{cm} is calculated based on the compressor absorbed power P_{cm} and the voltage at the compressor terminals, which is the FCS voltage V_{st}. The compressor absorbed power P_{cm} is calculated using nonlinear compressor maps [9]. The stack voltage V_{st} is a function of temperature, partial pressure of hydrogen and oxygen, and the stack current I_{st} [9]. Both P_{cm} and V_{st} can be expressed as a function of the net current I_{ref} at steady state. The FCS output power, calculated using

$$P_{fcs} = V_{st} I_{ref} \text{ [W]} \tag{10}$$

generated from the FCS model [8] is shown in Fig. 2. The FCS power output has a maximum $P_{fcs} \approx 54$ kW at $I_{ref} = 248$ A, due to the increasing losses. The FCS reference current is, therefore, limited to $I_{ref} \leq I_{ref}^{max} = 248$ A throughout this study. The average FCS efficiency for an entire drive cycle is defined as

$$\bar{\eta}_{fcs} = \frac{E_{fcs}}{E_{H_2}} \tag{11}$$

where E_{fcs} is the total energy out from the FCS and E_{H_2} is the total energy in the used fuel

Table 1 Vehicle model parameters

Mass (without battery) (m_0)	1384 kg
Rolling resistance coefficient (K_f)	0.02
Aerodynamic drag coefficient (C_d)	0.312
Frontal area (A)	2.06 m^2

Table 2 FCS model parameters

Cells (n_{cell})	381
Maximum net power (P_{fcs}^{max})	54 kW
Auxiliary power (fixed) (P_{aux})	500 W
Faraday's constant (F)	9.6485×10^{4}
Hydrogen molar mass (M_{H_2})	2.016×10^{-3} kg/mol
Hydrogen energy content ($Q_{HHV}^{H_2}$)	141.9×10^{6} J/kg
Gasoline energy content (Q_{HHV}^{gas})	46.7×10^{6} J/kg
Gasoline density (ρ_{gas})	733.22 kg/m^3

$$E_{fcs}=\int_0^T (P_{fcs}-P_{aux})dt \text{ [J]} \tag{12}$$

$$E_{H_2}=Q_{HHV}^{H_2}\int_0^T W_{H_2}dt \text{ [J]} \tag{13}$$

The parameters in the FCS model are shown in Table 2.

2.1.4 Battery Pack. The battery pack consists of multiple modules, which are modeled as a voltage source in series with a resistance and based on an ADVISOR model [10]. The battery output/input power P_{btt}, which is the remaining power to meet the drive-cycle power demand, is

$$P_{btt}(t)=P_{acc}(t)+P_{reg}(t)-[P_{fcs}(t)-P_{aux}] \text{ [W]} \tag{14}$$

where P_{acc} is the acceleration power demand (4), $(P_{fcs}-P_{aux})$ is the FCS net output power, and P_{reg} is the electric energy produced by the regenerative braking (6). When a load or power source is connected to the battery pack the battery current I_{btt} will depend on the power that is drawn/supplied from/to the pack

$$I_{btt}(\text{SoC},P_{btt})=\frac{V_{oc}(\text{SoC})-\sqrt{V_{oc}^2(\text{SoC})-4R_{int}(\text{SoC})P_{btt}}}{2R_{int}(\text{SoC})} \text{ [A]} \tag{15}$$

where V_{oc} is the open circuit voltage of the battery and R_{int} is the battery's internal resistance. The open-circuit voltage and the internal resistance are functions of the state of charge and the number of modules used in the battery pack. The open-circuit voltage and the internal resistance for a single module are shown in Fig. 3. The battery's state of charge (SoC) is calculated using

$$\frac{d}{dt}[\text{SoC}(t)]=\frac{-I_{btt}(t)\,\eta_{btt}[I_{btt}(t)]}{3600q_{btt}} \tag{16}$$

where η_{btt} is the battery charging efficiency

$$\eta_{btt}(I_{btt})=\begin{cases}1.0 & I_{btt}\geq 0\\ 0.9 & I_{btt}<0\end{cases} \tag{17}$$

and q_{btt} is the battery capacity. The parameters in the battery model are shown in Table 3.

Table 3 Battery model parameters

Mass (m_{btt})	6.68 kg
Capacity (q_{btt})	18 Ahr
Maximum output power (SoC=0.6)	2.78 kW
Charging efficiency (η_{btt}, $I_{btt}<0$)	0.9
SoC reference (SoC_{ref})	0.6

To determine the optimal operating point of the battery's SoC, a worst-case efficiency is calculated for the battery pack. The efficiency is calculated, using a discretized version of (16), in two separate cases. First, when the battery pack is first discharged from an initial given SoC, SoC(0), to a lower SoC, $\text{SoC}_{dis}(1)$, and then charged back to the initial SoC, SoC(2)=SoC(0)

$$\text{SoC}(0)\underset{P_{btt}^{dis}}{\rightarrow}\text{SoC}_{dis}(1)\underset{P_{btt}^{chg}}{\rightarrow}\text{SoC}(2)=\text{SoC}(0) \tag{18}$$

Second, when the battery pack is charged from the initial SoC, SoC(0), to a higher SoC, $\text{SoC}_{chg}(1)$, and then discharged back to the initial SoC, SoC(2)=SoC(0)

$$\text{SoC}(0)\underset{P_{btt}^{chg}}{\rightarrow}\text{SoC}_{chg}(1)\underset{P_{btt}^{dis}}{\rightarrow}\text{SoC}(2)=\text{SoC}(0) \tag{19}$$

The battery's worst-case efficiency is then given by

$$\eta_{btt}^{wc}=\frac{P_{btt}^{dis}}{P_{btt}^{chg}} \tag{20}$$

The resulting efficiency for a single module is shown in Fig. 4, where the left part is when first charging the battery, the right part is when first discharging, and the dashed lines are the maximum power output of the battery given by the SoC

$$P_{btt}^{dis}|_{max}=\frac{V_{oc}^2(\text{SoC})}{4R_{int}(\text{SoC})} \text{ [W]} \tag{21}$$

A 30% worst-case battery efficiency occurs, for example, when discharging the module with $P_{btt}^{dis}=2$ kW from SoC=0.5 and implies that the charging power required to charge the battery back to the initial SoC=0.5 is $P_{btt}^{chg}=6.6$ kW. Figure 4 shows that the optimal set point for the SoC is 0.6 because of the higher efficiencies for a wider range of discharging levels. The value 0.6 is also a good value because there is room for deviations without reaching too high or too low SoC levels. The initial condition of the SoC is therefore set to $\text{SoC}(0)=\text{SoC}_{ref}=0.6$ throughout this study. The input power, i.e., charging current, to the battery has not been limited, and all the charging power is assumed to be absorbed by the battery.

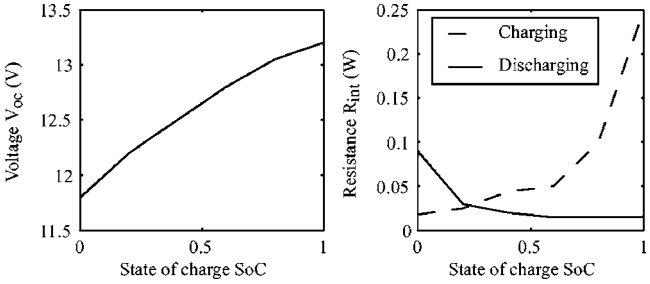

Fig. 3 Battery model characteristics: The open-circuit voltage (left) and internal resistance (right) both when charging (dashed line) and when discharging (solid line)

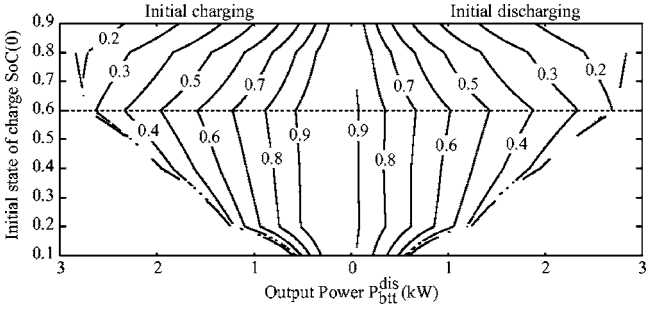

Fig. 4 Worst-case efficiency η_{btt}^{wc} (solid line), the maximum discharging output power $P_{btt}^{dis}|_{max}$ (dashed line), and the optimal SoC reference (dotted line) for different initial state of charge and discharging output power

Table 4 Drive-cycle characteristics and the power characteristics when $n_{btt}=10$ and $m=1451$ kg

Cycle	NYCC	FTP-72	SFTP
Average power			
Acc. (kW)	4.9	7.2	21.5
Brk. (kW)	4.1	7.0	17.3
Max power			
Acc. (kW)	25.7	31.8	80.1
Brk. (kW)	21.6	23.4	53.8
Top speed (km/hr)	44.6	91.3	129.2
Duration (s)	599	1370	601
Distance (m)	1898	11,990	12,888
$E_{acc}^{m_0}$ (33) (MJ)	1.024	5.748	8.980

2.2 Drive Cycles. The power demand from the drive cycles is calculated backward using the discretized version of the vehicle model (1). Note that the power demand will therefore differ from models, including a driver model driving, driving on the same cycles. The three drive cycles used are New York City cycle (NYCC), which represents low-speed and mild driving; federal test procedure-72 cycle (FTP-72) which represents both low-speed city driving and moderate highway driving; and supplemental federal test procedure cycle (SFTP), which represents aggressive high-speed driving. The drive cycles and their power characteristics for a vehicle with ten battery modules and a mass of 1451 kg are summarized in Table 4.

2.3 Dynamic Programming. The DP methodology [7] can be used to numerically solve optimal control problems. We will, in this study, use deterministic DP to optimize the battery size separately for different drive cycles to show the drive cycle's effect on the battery sizing. The FCHEV model can be described as the nonlinear state space model

$$\dot{x} = f_t(x,u,w) \tag{22}$$

with the state $x=\mathrm{SoC}$ from (16), the reference current as the input $u=I_{\mathrm{ref}}$, and the power demand as the disturbance $w=P_{\mathrm{dem}}$. The second state, v, in the model is not included when using the DP because the power demand is precalculated using the vehicle model (1). The known power demand throughout the cycle allows the application of DP to calculate backward (noncausally) the optimal input $u=I_{\mathrm{ref}}$ sequence as it is clarified below.

Forward Euler approximation, with a sampling interval of 1 s, is used to derive the discrete-in-time representation of the FCHEV,

$$x_{k+1} = f(x_k,u_k,w_k) + x_k \tag{23}$$

The variables x_k, u_k, and w_k are limited to the finite spaces X, U, and W with $x_k \in X$, $u_k \in U$, $w_k \in W$. The DP algorithm allows us to find the control sequence $u=(u_o,\ldots,u_{k-1})$ that minimizes the cost function

$$\sum_{\tau=0}^{\tau=K} J(x_\tau,u_\tau) \rightarrow \min \tag{24}$$

where $J(x_\tau,u_\tau)$ is the cost to use the input u_τ at the state x_τ. The cost J is defined as

$$J = (\alpha \Delta\mathrm{SoC})^2 + \beta W_{\mathrm{H}_2} \tag{25}$$

$$\Delta\mathrm{SoC} = \mathrm{SoC} - \mathrm{SoC}_{\mathrm{ref}} \tag{26}$$

where ΔSoC is the deviation of the battery's state of charge from the reference value $\mathrm{SoC}_{\mathrm{ref}}$, W_{H_2} is the hydrogen consumption in the FCS, and $\{\alpha,\beta\}$ are weights. The battery model does not consider deterioration of the battery, which is associated with repetitive large charging and discharging. Therefore, we penalize large SoC deviation heavily, hence the quadratic penalty of ΔSoC, to consider battery deterioration. The weights α and β in (25) are set so that when $\Delta\mathrm{SoC}=0.1$ and $W_{\mathrm{H}_2}=W_{\mathrm{H}_2}(I_{\mathrm{ref}}^{\max})=0.0013$ kg/s then $(\alpha\Delta\mathrm{SoC})^2=\beta W_{\mathrm{H}_2}=J/2=1$, i.e., each performance variable contributes equally to the cost when the SoC deviation is 0.1 and the FCS is operating at maximum level.

To solve the optimal control problem (24), we need to define an intermediate problem that starts at time k with an initial state x_k. Let us define $V(x_k,k)$ the optimal cost-to-go or value function that will be incurred if the system starts at state x_k at time k and continues to the final time K

$$V(x_k,k) = \min_{u(k),u(k+1),\ldots,u(K-1)} \sum_{\tau=k}^{\tau=K-1} J(x_\tau,u_\tau,w_\tau) \tag{27}$$

with the final penalty $V(x_K,K)=(\delta\Delta\mathrm{SoC})^2$, $\delta=10^3$. The final state x_K at time K is penalized to ensure that the final state of charge is close to the initial state of charge. We then obtain a relationship that relates the value function at a certain point in time to the value function at a later point in time. Let x_m be the state at time m, and suppose that $(u_m,u_{m+1},\ldots,u_{K-1})$ is a given control sequence that generates the trajectory $x_m,x_{m+1},\ldots,x_K$. Let l be anytime instance that satisfies $m<l\leq K-1$. The value function satisfies

$$\begin{aligned} V(x_m,m) &= \sum_{\tau=m}^{\tau=l-1} J(x_\tau^*,u_\tau^*) + V(x_l^*,l) \\ &= \min_{u(m),\ldots,u(l-1)} \left(\sum_{\tau=m}^{\tau=l-1} J(x_\tau,u_\tau) + V(x_l,l) \right) \end{aligned} \tag{28}$$

which is the principle of optimality. In other words if $u_m^*,\ldots,u_l^*,\ldots,u_{K-1}^*$ is optimal for the problem starting at $k=m$ and $x_m^*,\ldots,x_l^*,\ldots,x_K^*$ is the resulting trajectory, then $u_l^*,\ldots,u_{K-1}^*$ is optimal for the problem that starts at $k=l$ with initial condition x_l^*. Finally, consider $m=k-1$ and $l=k$, then the Bellman equation [7] is obtained

$$V(x_{k-1},k-1) = \min_{u_{k-1}} [J(x_{k-1},u_{k-1}) + V(x_k,k)] \tag{29}$$

which allows the calculation of the optimal control sequence backwards starting from $k=K$.

The grid of the finite discrete state spaces X, U, and W has been chosen depending on the drive cycle and battery size of the optimization. The grid has been chosen with nonregular spacing at several regions to accommodate, for example, SoC levels close to the reference $\mathrm{SoC}_{\mathrm{ref}}$ better than SoC levels far from the SoC reference. For more technicalities on the algorithm and the grid, see [11].

Before the DP optimization results are presented, it is important to note that these results depend on the cost selection (25), and their sensitivity to this cost selection has not been studied yet.

3 Dynamic Programming Results

This section shows the results from the DP optimizations. We will focus on the energy losses in the different components and how they change with the battery size. These results are separated into two parts. First, without regenerative braking and second, when including regenerative braking with various efficiencies.

3.1 Without Regenerative Braking. To observe if hybridization can be beneficial when the objective is only to decouple the power demand between the traction motor and the fuel cell, we first present the results when the regenerative braking efficiency is $\eta_{\mathrm{reg}}=0\%$. We will show how and why the FCS efficiency changes

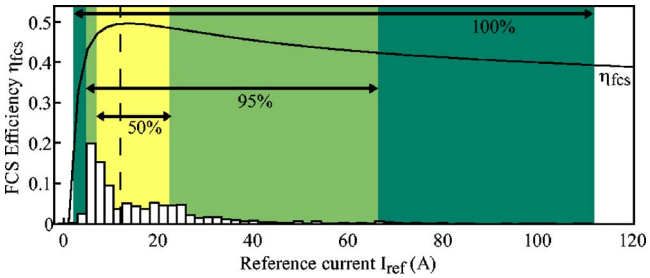

Fig. 5 FCS reference current I_{ref} distribution and the FCS efficiency η_{fcs} for a vehicle with ten modules for the medium (FTP-72) drive cycle. The median value of the reference current is shown with dashed line together with the regions (50%, 95%, and 100%) around this median.

when increasing the battery size. Moreover, the energy expended by charging/discharging the battery and the energy lost due to added weight with increasing battery size are shown.

3.1.1 Fuel Cell System. An example of how DP uses the FCS for a vehicle with ten battery modules for the medium drive cycle is shown in Fig. 5. Under these conditions, 50% of the reference current values are between 7 A and 22 A, 95% between 4.7 A and 66 A, and 100% between 2 A and 111 A. The resulting average FCS efficiency (11) for this configuration is 46.1%. The average FCS efficiency for different battery sizes is shown in the left column of Fig. 6. When increasing the battery size the average FCS efficiency increases. This increase is accomplished through the decoupling between the acceleration power demand P_{acc}, and the FCS output power P_{fcs}. In particular, the right column of Fig. 6 shows that the FCS operates more often at reference current levels with higher efficiency. The right column of Fig. 6 shows the distribution regions of the FCS reference current for different

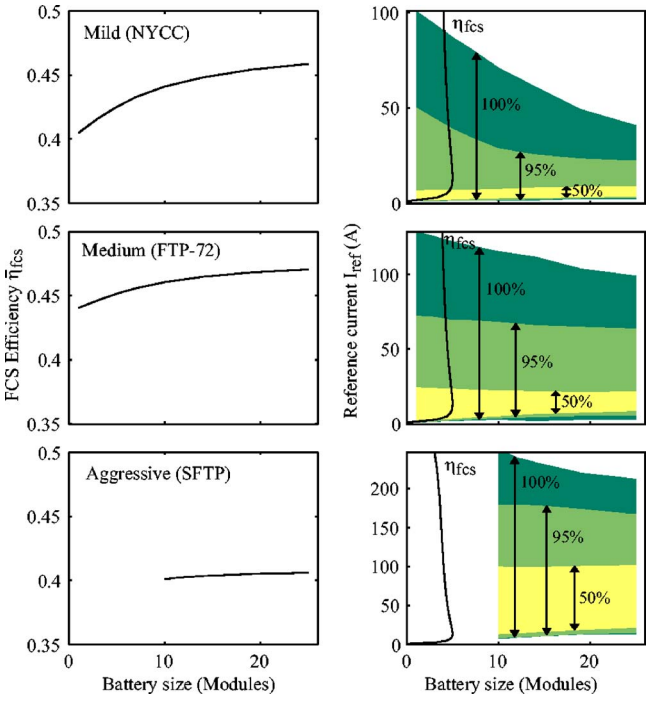

Fig. 6 Average FCS efficiency $\bar{\eta}_{fcs}$ (left) together with the reference current distribution (right) for different battery sizes and drive cycles (without regenerative braking). The FCS efficiency curve is shown in the left part of the reference current distribution plot.

sizes together with the FCS efficiency curve (8). Note that the graphs in the right column of Fig. 6 condense the information in Fig. 5 (switched axes) for different battery sizes.

For the mild cycle, the FCS operates at low current levels and adding battery modules improves the FCS efficiency. In fact, the FCS efficiency improvement observed in the mild cycle is the largest of all cycles. The FCS efficiency improvements are, for all cycles, realized by both a shift of low current levels to higher and a shift of high current levels to lower. The significant improvement in the mild cycle can be explained as follows. More than 50% of the reference current levels is at the low levels below the optimal FCS current level. Operating the FCS with very low currents is very inefficient, due to parasitic losses; thus, there is a large increase in FCS efficiency when DP stores energy in the battery and shifts the low current levels drawn from the FCS toward higher current regions. For the medium cycle, there is less need for operation in the low efficient region of very small currents. The vehicle will therefore not benefit as much as for the mild cycle when increasing the battery size. Note that at least ten battery modules are needed to satisfy the acceleration demand in the aggressive cycle.

3.1.2 Battery. The electrical energy expended in the battery[2] is defined as

$$E_{loss}^{btt} = \left| \int_0^T P_{btt} dt \right| \ [\mathrm{J}] \tag{30}$$

where P_{btt} is the battery power. To be able to compare the total energy loss in the vehicle and the expended energy in the battery, we need to define the hydrogen equivalent energy $E_{loss}^{btt}/\bar{\eta}_{fcs}$. This is the hydrogen energy required to produce the electric energy expended in the battery. The energy expended in the battery, E_{loss}^{btt} together with the hydrogen equivalent energy, $E_{loss}^{btt}/\bar{\eta}_{fcs}$, is shown in the left column of Fig. 7.

It is not easy to analyze the trend between the energy expended in the battery and the battery size for the different cycles. The difficulty arises because the power split is decided through the DP policy and not through a rule-based controller. Specifically, the DP uses the battery to save some energy by allowing the FCS to operate more efficiently and will waste some of this energy in the battery.

3.1.3 Added Mass. The energy loss due to the added mass, when increasing the battery size, affects the performance of the vehicle. It is therefore important to separate the losses due to the added weight from the other losses. We define the energy loss due to the added weight as

$$E_{loss}^{\Delta m} = E_{acc}^{m} - E_{acc}^{m_0} \ [\mathrm{J}] \tag{31}$$

$$E_{acc}^{m} = \int_0^T P_{acc}(m_0 + n_{btt} m_{btt}, t) dt \ [\mathrm{J}] \tag{32}$$

$$E_{acc}^{m_0} = \int_0^T P_{acc}(m_0, t) dt \ [\mathrm{J}] \tag{33}$$

where $P_{acc}(m_0)$ is the acceleration power demand (4) for a vehicle without any battery and $P_{acc}(m_0+n_{btt}m_{btt})$ is the acceleration power demand for a vehicle with n_{btt} battery modules. The parameters m_0 and m_{btt} are shown in Tables 1 and 3. The energy loss due to the added mass $E_{loss}^{\Delta m}$ and the hydrogen equivalent energy loss $E_{loss}^{\Delta m}/\bar{\eta}_{fcs}$ are shown in the right column of Fig. 7. The energy loss $E_{loss}^{\Delta m}$ is increasing proportional to the battery size for all three

[2]Note that even though the DP ensures that $SoC(T) \approx SoC(0)$, there is always energy expended in the battery ($E_{loss}^{btt} > 0$) due the internal resistance and the charging efficiency, η_{btt} (17).

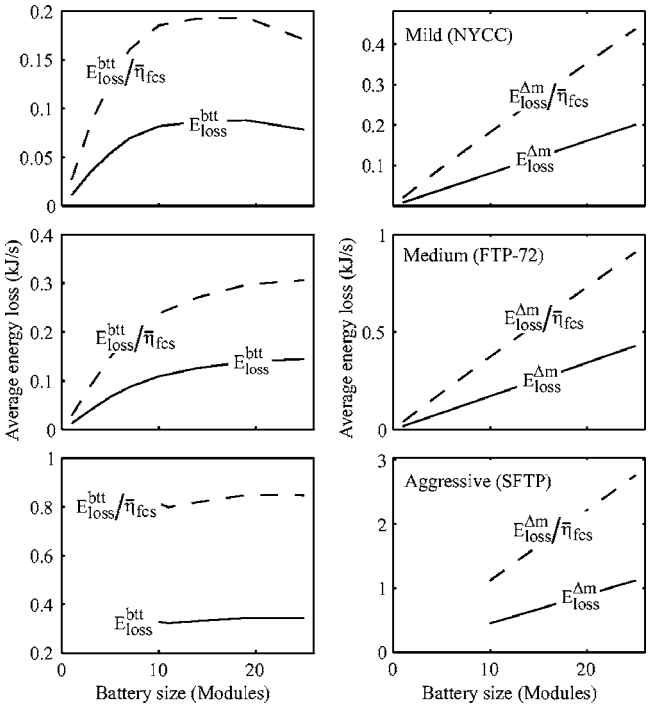

Fig. 7 Average expended electric energy in the battery and its hydrogen equivalent energy (left) together with the average electric energy loss due to the added mass and its hydrogen equivalent energy loss (right) without regenerative braking

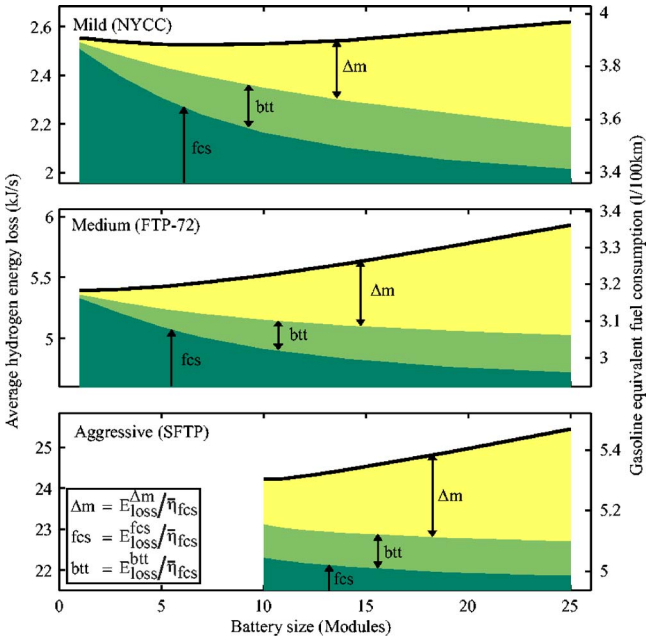

Fig. 8 Average hydrogen equivalent energy loss per second and its origins in the three drive cycles for different battery sizes (without regenerative braking). The solid line shows the gasoline equivalent fuel consumption.

drive cycles. The hydrogen equivalent energy loss is increasing slightly faster for smaller battery sizes for the mild and medium drive cycles due to the changing FCS efficiencies in Fig. 6. Note that an increase in battery size corresponds to an increase in vehicle weight *and* net vehicle power because the FCS power size remains fixed.[3]

3.1.4 System. To compare the expended energy in the battery and the energy losses due to the added weight to the remaining losses in the FCS, we define the total hydrogen energy loss for a cycle

$$E^0_{\text{loss}} = E_{\text{H}_2} - E^{m_0}_{\text{acc}} \text{ [J]} \tag{34}$$

where E_{H_2} is the total energy in the used fuel (13) and $E^{m_0}_{\text{acc}}$ is the energy defined in (33). The total hydrogen energy loss can be separated into three parts

$$E^0_{\text{loss}} = \frac{E^{\text{fcs}}_{\text{loss}}}{\bar{\eta}_{\text{fcs}}} + \frac{E^{\text{btt}}_{\text{loss}}}{\bar{\eta}_{\text{fcs}}} + \frac{E^{\Delta m}_{\text{loss}}}{\bar{\eta}_{\text{fcs}}} \tag{35}$$

where $E^{\text{btt}}_{\text{loss}}/\bar{\eta}_{\text{fcs}}$ is the hydrogen equivalent energy expended in the battery, $E^{\Delta m}_{\text{loss}}/\bar{\eta}_{\text{fcs}}$ is the hydrogen equivalent energy loss due to the added mass, and $E^{\text{fcs}}_{\text{loss}}/\bar{\eta}_{\text{fcs}}$ is the remaining hydrogen equivalent energy loss in the FCS.[4] The electric energy expended in the battery $E^{\text{btt}}_{\text{loss}}$ is defined in (30), and the electric energy loss due to added weight is defined in (31). The remaining electric energy loss in the FCS is then calculated using

$$E^{\text{fcs}}_{\text{loss}} = \bar{\eta}_{\text{fcs}} E^0_{\text{loss}} - E^{\text{btt}}_{\text{loss}} - E^{\Delta m}_{\text{loss}} \text{ [J]} \tag{36}$$

where $\bar{\eta}_{\text{fcs}} E^0_{\text{loss}}$ can be seen as the total electric energy lost. The total hydrogen energy loss E^0_{loss} is proportional to the total hydrogen mass consumption and, therefore, to the gasoline equivalent fuel consumption[5]

$$C^V_{\text{gas}} = 10^8 \frac{E^0_{\text{loss}} + E^{m_0}_{\text{acc}}}{Q^{\text{gas}}_{\text{HHV}} \rho_{\text{gas}} \int_0^T v dt} \left[\frac{1}{100 \text{ km}}\right] \tag{37}$$

where $Q^{\text{gas}}_{\text{HHV}}$ is the energy content of gasoline (based on the higher heating value), ρ_{gas} is the gasoline density (Table 2), and $\int_0^T v dt$ is the total distance covered during the cycle (Table 4).

The energy losses in (35) together with the gasoline equivalent fuel consumption C^V_{gas} are shown in Fig. 8. For the mild cycle, the large increase in FCS efficiency at first reduces the total energy loss when increasing the battery size. For larger battery sizes, though, the loss due to the added weight increases more than the other losses decreases. Therefore, the mild cycle has an optimal battery size of around five modules. For the medium cycle, the FCS efficiency does not increase enough to compensate for the added weight and there is therefore no point in adding a battery to the vehicle. In the aggressive cycle, there is a minimum battery size of ten modules to meet the high power demand (Table. 4). However, there is no reduction in the total energy lost due to the increasing energy lost due to the added battery weight. Thus, to the contrary of hybridizing an ICE vehicle, hybridization of a fuel cell vehicle cannot always be justified based solely on fuel consumption improvements.

3.2 With Regenerative Braking. This section shows the DP results when the regenerative braking efficiency η_{reg} is varied between 0% and 50%. We will show how the regenerative braking affects the energy losses in the battery and, hence, the battery sizing. An attempt to determine the amount of expended energy in

[3]Note here that it would have been more meaningful to perform this investigation with a fixed vehicle net power and varying the power split ratio between the FCS and the battery. A scalable FCS model with accurate parasitic losses that allows the power split ratio to be varied is, however, not available.

[4]Since $E^{\Delta m}_{\text{loss}}$ is the energy lost due to the *added* mass, the energy $E^{\text{fcs}}_{\text{loss}}$ includes both the electric energy lost in the FCS and the electric energy lost when providing the acceleration energy $E^{m_0}_{\text{acc}}$. However, we will show these as one throughout this study.

[5]The US fuel economy, measured in miles per gallon, is $C^V_{\text{gas}}|_{\text{US}} \approx 235.2\ (C^V_{\text{gas}})^{-1}$ mpg.

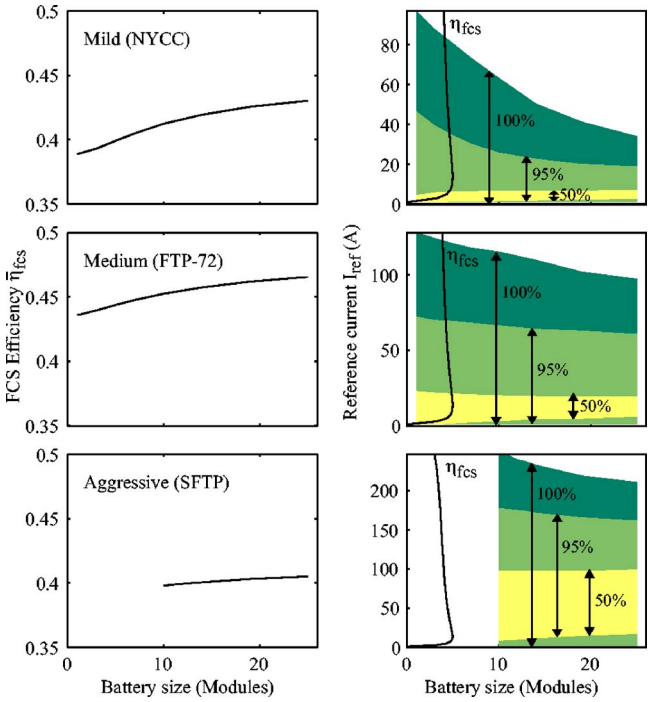

Fig. 9 Fuel cell system efficiency $\bar{\eta}_{fcs}$ (left) together with the reference current distribution (right) for different battery sizes and drive cycles (with 50%regenerative braking). The FCS efficiency curve is shown in the left part of the reference current distribution plot.

the battery that is associated with the regenerative braking and how much is associated with improving the performance of the FCS is presented. First, a similar approach, as in Sec. 3.1, is used to describe the different components contribution to the overall energy loss for a vehicle where the regenerative braking transfers 50% of the braking power to the battery pack. Second, a description of the energy losses and their behavior when the regenerative braking efficiency is increased from 0% to 50% is shown in a compressed format.

3.2.1 Fuel Cell System. The FCS efficiency (11) is shown in the left column of Fig. 9. When increasing the battery size, the FCS efficiency increases. This increase is caused, as the case in Sec. 3.1, by decoupling the acceleration power demand P_{acc} from the fuel cell output power P_{fcs}. The right column of Fig. 9 shows the distribution of the FCS reference current I_{ref}, for different sizes together with the FCS efficiency curve η_{fcs} (8). The changes of these distributions are similar to those in Sec. 3.1. When increasing the battery size, the DP shifts the inefficient current levels toward higher efficiencies. The average FCS efficiencies achieved now are lower than the ones observed in previous sections because the regenerative braking causes the expended energy in the battery to increase and thus reducing the room for an FCS efficiency increase by using the battery. As in previous sections, when not considering regenerative braking, the peak reference current now shifts to lower values with high FCS efficiency as shown in Fig. 9 (right column) and the low reference current shift toward higher regions.

3.2.2 Battery. Without regenerative braking, the entire energy expended in the battery was caused by the FCS charging and improving its efficiency. When including the regenerative braking, however, we need to separate the energy expended in the battery caused by the charging through regenerative braking and the expended energy caused by the charging through the FCS. Therefore, we define the regenerative braking power used to charge the battery

$$P_{btt}^{chg}|_{reg} = \begin{cases} P_{reg} & P_{fcs} - P_{aux} > 0 \\ P_{reg} - (P_{fcs} - P_{aux}) & P_{fcs} - P_{aux} \le 0 \end{cases} \text{[W]} \quad (38)$$

where P_{reg} is the regenerative braking power, P_{fcs} is the FCS output power, and P_{aux} is the auxiliary power demand. The total regenerative braking energy used to charge the battery is then

$$E_{btt}^{chg}|_{reg} = \int_0^T (P_{btt}^{chg}|_{reg})dt \text{ [J]} \quad (39)$$

The total power, including both the regenerative braking and the FCS, used to charge the battery is the negative part of the battery power P_{btt}

$$P_{btt}^{chg} = \begin{cases} 0 & P_{btt} > 0 \\ |P_{btt}| & P_{btt} \le 0 \end{cases} \text{[W]} \quad (40)$$

where P_{btt} is defined in (14). The total energy used to charge the battery is

$$E_{btt}^{chg} = \int_0^T (P_{btt}^{chg})dt \text{ [J]} \quad (41)$$

The regenerative braking fraction of the energy used to charge the battery is defined

$$\theta_{btt}^{chg}|_{reg} = \frac{E_{btt}^{chg}|_{reg}}{E_{btt}^{chg}} \quad (42)$$

By analogy, we postulate that the fraction $\theta_{btt}^{chg}|_{reg}$ distinguishes the energy expended in the battery that is caused by the regenerative braking from the expended battery energy, which is caused by the FCS. The expended battery energy caused by the regenerative braking is

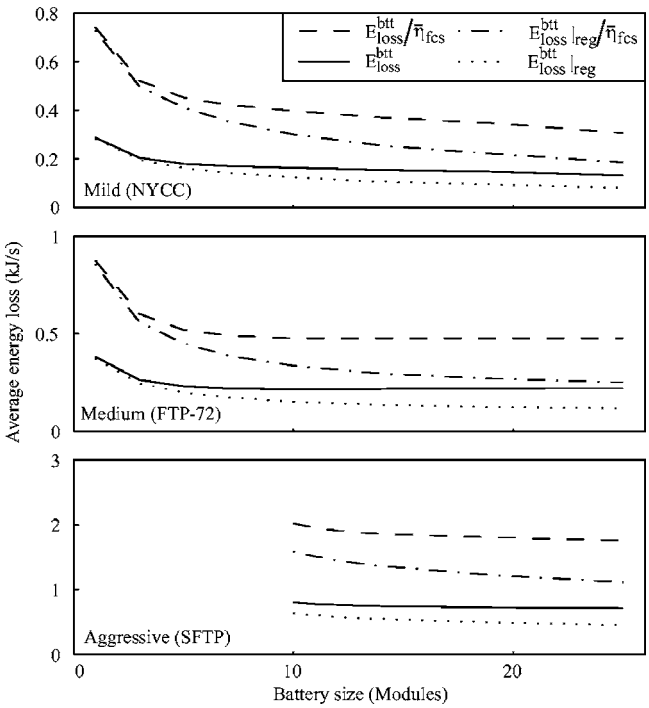

Fig. 10 Average energy expended in the battery and its hydrogen equivalent energy together with expended energy in the battery due to the regenerative braking and its hydrogen equivalent energy (with 50% regenerative braking)

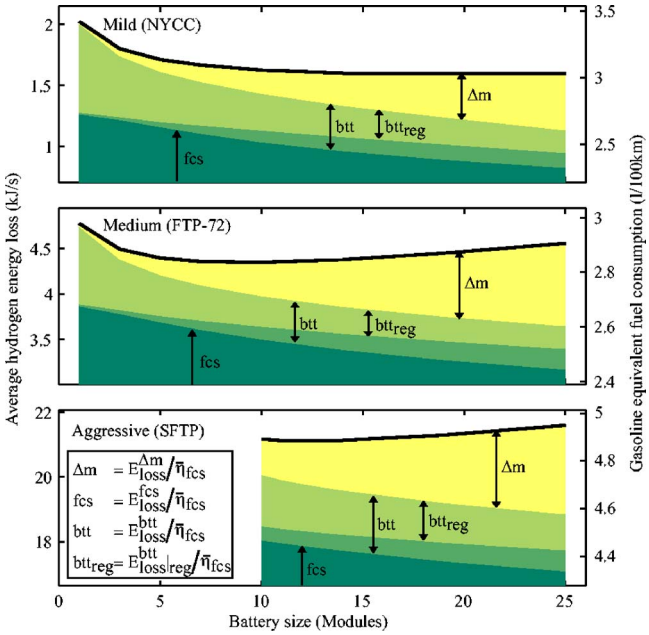

Fig. 11 Average hydrogen equivalent energy loss per second and its origins in the three drive cycles for different battery sizes (with 50% regenerative braking). The solid line shows the gasoline equivalent fuel consumption.

$$E_{\text{loss}}^{\text{btt}}|_{\text{reg}} = \theta_{\text{btt}}^{\text{chg}}|_{\text{reg}} E_{\text{loss}}^{\text{btt}} \text{ [J]} \tag{43}$$

and the remaining expended battery energy caused by the FCS is

$$E_{\text{loss}}^{\text{btt}}|_{\text{fcs}} = (1 - \theta_{\text{btt}}^{\text{chg}}|_{\text{reg}}) E_{\text{loss}}^{\text{btt}} \text{ [J]} \tag{44}$$

where the expended battery energy $E_{\text{loss}}^{\text{btt}}$ is defined in (30).

Figure 10 shows the average total energy expended (solid) in the battery pack together with its hydrogen equivalent energy (dashed line) for a vehicle with a regenerative braking efficiency of 50%. Moreover, Fig. 10 shows the expended energy in the battery caused by regenerative braking charging (dotted) and its hydrogen equivalent energy (dashed-dotted line). Note that, for small battery sizes, all of the expended energy is caused by regenerative braking. Furthermore, the expended energy caused by the FCS charging, which is the difference between the total expended energy and the expended energy caused by regenerative braking charging, has a similar increase when increasing the battery size as when disregarding regenerative braking.

3.2.3 Added Mass. The energy losses due to the added mass are similar to those when disregarding regenerative braking (right column of Fig. 7) since the energy $E_{\text{loss}}^{\Delta m}$ (31), is independent from the regenerative braking.

3.2.4 System. For a vehicle with a regenerative braking efficiency of 50%, the total hydrogen energy loss, the hydrogen equivalent energy loss due to the added weight, and the hydrogen equivalent energy expended in the battery are shown in Fig. 11. The energy expended in the battery $E_{\text{loss}}^{\text{btt}}$ is separated in expended energy caused by the regenerative braking, $E_{\text{loss}}^{\text{btt}}|_{\text{reg}}$, and the expended energy caused by the FCS $E_{\text{loss}}^{\text{btt}}|_{\text{fcs}}$. For the mild cycle, the large energy expended in the battery for small battery sizes together with the large energy loss due to the added weight for large batteries generate an optimal battery size of 14–20. For the medium cycle the optimal battery size is nine modules. In the aggressive cycle, the decrease in expended battery energy is almost equivalent to the energy loss due to added weight. However, there is an optimal battery size of 12 modules.

3.3 Varied Regenerative Braking Efficiency. Because it is challenging to estimate the efficiency of the regenerative braking and because $\eta_{\text{reg}}=50\%$ is an optimistic estimate of what can be practically achieved, the regenerative braking efficiency has been varied between 0% and 50%.

Figure 12 shows the different energy losses for the different drive cycles when the regenerative braking efficiency is varied from 0% to 50%. Even though all the energy expended in the battery is caused by the regenerative braking for small sizes, the overall energy loss is decreased (compare Figs. 8 and 12), making regenerative braking a desirable option when a battery pack is included in the vehicle.

The energy expended in the battery due to the FCS is similar to the energy expended in the battery when not considering the regenerative braking (Sec. 3.1). This expended energy is decreasing when increasing the regenerative braking efficiency because the

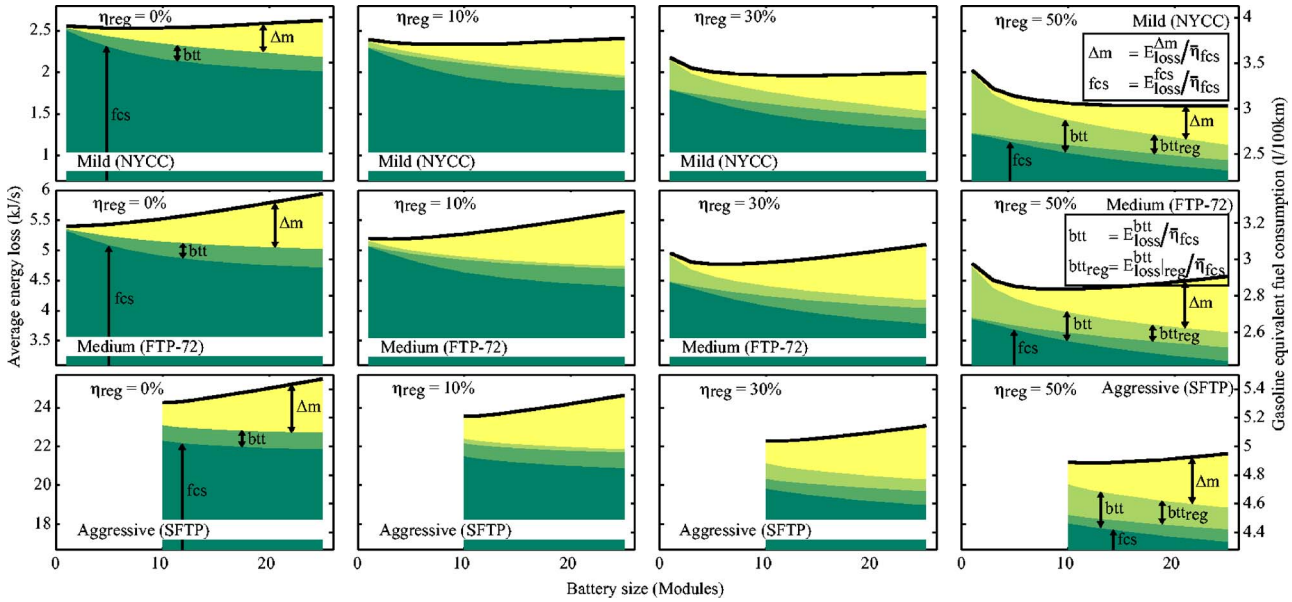

Fig. 12 Average hydrogen equivalent energy loss per second and its origins in the three drive cycles for different battery sizes with regenerative braking efficiencies of 0% to 50%. The solid line shows the gasoline equivalent fuel consumption.

braking increases the battery activity, and there is, therefore, less opportunity to use the battery by the FCS to increase its efficiency. The optimal battery sizes for all three drive cycles are increasing when the regenerative braking efficiency is increasing, even though for the aggressive cycle, the optimal battery size is 12 modules when $\eta_{reg}=50\%$, and the minimum is ten modules when $\eta_{reg}=0\%$. The total energy loss, as expected, decreases when the regenerative braking efficiency increases but as can be seen for the medium cycle in Fig. 12, a vehicle with 25 battery modules and $\eta_{reg}=30\%$ can generate the same total energy loss as a vehicle with three modules and $\eta_{reg}=10\%$. This emphasizes the importance of the battery sizing issue while designing FCHEVs.

4 Conclusions and Future Work

For the considered vehicle, fuel cell system, and battery, this study shows that during hybridization the energy loss due to the extra weight can exceed the improvements in FCS efficiency. Though, when the considered vehicle is solely driving in a mild cycle with low speed, there are indications that the fuel consumption could be lowered by hybridization. These improvements are accomplished by eliminating the need for operating the FCS at extremely low reference currents where the FCS auxiliary losses are dominant similarly to what was discovered experimentally in [12]. If the vehicle is solely driving at low speed, it is possible that the fuel consumption could be lowered through decreasing vehicle weight by downsizing the FCS and excluding the battery pack since the mild cycle would appear more aggressive for a smaller FCS. This, however, requires a more comprehensive study of FCS hybridization in city vehicles. For the aggressive drive cycle, the minimum battery size was ten modules because the high power demand could not be met by the considered FCS alone. Note that if a scalable FCS model was available, the need for hybridization in the aggressive cycle could possibly change.

We can see throughout this study that hybridization offers a greater benefit for the mild (NYCC) drive cycle than for the medium (FTP-72) and aggressive (SFTP) drive cycles, regardless, if including the regenerative braking or not. These results match the results shown in [1].

When regenerative braking is considered, the battery is forced to absorb the associated energy. An increase in regenerative braking efficiency will increase the energy expended in the battery, especially for small sizes, and therefore increase the optimum battery size. The overall fuel consumption decreases when including regenerative braking. For the considered vehicle with 50% regenerative braking efficiency, the optimal battery size is between 10 and 15 modules for all three drive cycles.

The optimal battery size is dependent on the cycle, the vehicle weight, the type of battery, and energy density of the battery. Thus, this study is very specific to our configuration, the specific weights and characteristics of the vehicle, and its different components. Furthermore, the cost function when using DP influences, in general, the optimal results and, in particular, the optimal battery sizes in this study. Moreover, the model used in this study is very simple and does not consider mechanical losses in the power train. The results can however be seen as an indication of how the optimal battery size change when different levels of regenerative braking are introduced. The added weight is the factor that makes configurations with larger batteries perform worse; it is therefore crucial to increase the power-to-weight ratio of the batteries.

In future work this study could be performed under fixed vehicle net power by resizing battery and FCS simultaneously. Resizing the FCS depends on scalable FCS auxiliary losses and associated transient response.

Acknowledgment

This work is supported by the National Science Foundation Grant No. CMS-0201332 and the Automotive Research Center, with partial funding from Ford Motor Company.

References

[1] Friedman, D. J., 1999, "Maximizing Direct-Hydrogen PEM Fuel Cell Vehicle Efficiency—Is Hybridization Necessary," SAE Paper No. SP-1425.
[2] Matsumoto, T., Watanabe, N., Sugiura, H., and Ishikawa, T., 2002, "Development of Fuel-Cell Hybrid Vehicle," SAE Paper No. 2002-01-0096, SP-1691.
[3] Lin, C. C., Peng, H., and Grizzle, J. W., 2004, "A Stochastic Control Strategy for Hybrid Electric Vehicles," *Proc. of American Control Conference*, Boston, AACC & IEEE, New York, pp. 4710–4715.
[4] Ishikawa, T., Hamaguchi, S., Shimizu, T., Yano, T., Sasaki, S., Kato, K., Ando, M., and Yoshida, H., 2004, "Development of Next Generation Fuel-Cell Hybrid System—Consideration of High Voltage System," SAE Paper No. 2004-01-1304, SP-1827.
[5] Sundstrom, O., and Stefanopoulou, A., 2006, "Optimal Power Split in Fuel Cell Hybrid Electric Vehicle With Different Battery Sizes, Drive Cycles, and Objectives," "*Proc. of 2006 IEEE International Conference on Control Applications*, Munich, Germany, IEEE, New York, pp. 1681–1688.
[6] Jeong, K. S., and Oh, B. S., 2002, "Fuel Economy and Life-Cycle Cost Analysis of a Fuel Cell Hybrid Vehicle," J. Power Sources, **105**, pp. 58–65.
[7] Bellman, R. E., 1957. *Dynamic Programming*, Princeton University Press, Princeton.
[8] Suh, K.-W., and Stefanopoulou, A. G., 2006, "Effects of Control Strategy and Calibration on Hybridization Level and Fuel Economy in Fuel Cell Hybrid Electric Vehicle," SAE Paper No. 2006-01-0038.
[9] Pukrushpan, J. T., Peng, H., and Stefanopoulou, A. G., 2004, "Control-Oriented Modeling and Analysis for Automotive Fuel Cell Systems," ASME J. Dyn. Syst., Meas., Control, **126**, pp. 14–25.
[10] Johnson, V. H., 2002, "Battery Performance Models in Advisor," J. Power Sources, **110**, pp. 321–329.
[11] Sundstroem, O., 2006, "Optimal Power Split in Fuel Cell Hybrid Electric Vehicle With Different Battery Sizes, Drive Cycles, and Objectives," Master's thesis, Chalmers University of Technology, Gothenburg, Sweden.
[12] Rodatz, P., Paganelli, G., Sciarretta, A., and Guzzella, L., 2005, "Optimal Power Management of an Experimental Fuel Cell/Supercapacitor-Powered Hybrid Vehicle," Control Eng. Pract., **13**(1), pp. 41–53.